International Symposium
On Turbulence and Shear Flow
Phenomena (TSFP-8)
August 28 - 30, 2013 Poitiers, France

Characteristics Extraction of a Turbulent Diffusion State for Quick Trace-Back Estimation of the Diffusion Source

Kana OYAGI
Department of Mechanical Engineering
Tokyo University of Science
2641 Yamazaki, Noda-shi, Chiba-ken
j7512614@ed.tus.ac.jp

Takahiro TSUKAHARA, Yasuo KAWAGUCHI
Department of Mechanical Engineering
Tokyo University of Science
2641 Yamazaki, Noda-shi, Chiba-ken
tsuka@rs.noda.tus.ac.jp, yasuo@rs.noda.tus.ac.jp

ABSTRACT

When a severe accidents occurs and hazardous substance which damages the environment and public health is emitted into the atmosphere, it is necessary to pinpoint the source of diffusion and to take remedial measures immediately.

In order to develop a method of source location, we proposed and tested presumption strategy based on two kinds of experimental results of turbulent diffusion. The spatial distribution of turbulent velocity and concentration fluctuation was acquired by PIV/PLIF simultaneous measurement. Thereby, we tried to extract features which characterize a distance from a source which is useful to locate the source position from the position of observation.The next experiment was PLIF time series aquisition. This experimental record gave us concentration information which has high spatial and temporal resolution. Using these data, we examined two kinds of source presumption methods. One estimates the source position from instantaneous observation in wide area ; the other estimated short time statistical observation at limited positions. We compared these performances and considered their validity.

1. INTRODUCTION

In an incident in which pollution/harmful substances that might affect the environment and public health are emitted into the atmosphere, it is necessary to pinpoint the source of diffusion and take measures immediately. Previously, the world has seen a large number of victims from the diffusion accidents. Also in Japan, the radioactive material that was emitted from the Fukushima Daiichi nuclear power plant has brought the severe environmental pollution when the Great East Japan Earthquake occurred in 2011. Recently, requests for a diffusion source prediction method have been increasing because the number of potential diffusion sources is increasing due to the expansion of city regions and population growth in developing countries (Furuno et al., 2006).

Currently, when we have to understand a situation involving substance diffusion, the spatial and temporal concentration can be predicted by some forward analytical solutions based on the normal CFD method. In such an analysis, information on the source position and diffusion amount is necessary. However, when the serious accidents occur, this information is sometimes not known and then we will not have enough time to perform such an analysis. Therefore, a quick trace-back estimation method to detect the diffusion source from the observed value of diffused-substance (concentration) distribution in short duration is required. A number of methods have been developed to date. The back-trajectory method is widely used (Bagtzoglou et al., 1992). This method can calculate the solutions quickly by tracing back the movement of a particle. Also, there is another method which is based on the Gaussian plume model (Islam, 1999). Furthermore, the analytical technique is valid for a simple condition like a homogeneous flow (Kathirgamanathan, 2002). However, further research is required for impractical application because actual data that can be used as initial and boundary conditions in this method are limited. Considering the previous research, the concentration fluctuation accompanied by turbulent diffusion at high Reynolds numbers cannot be applied in the traditional trace back analysis. In this research, with the aim of evaluating the potential and the limitations of the source estimation in environmental diffusions with turbulent backgrounds, we have examined a sample concentration field with an emission point in a water channel flow as a test case.

2. EXPERIMENTAL APPARATUS

Our experimental apparatus was the closed circulated channel shown in Fig.1. Fully-developed two-dimensional

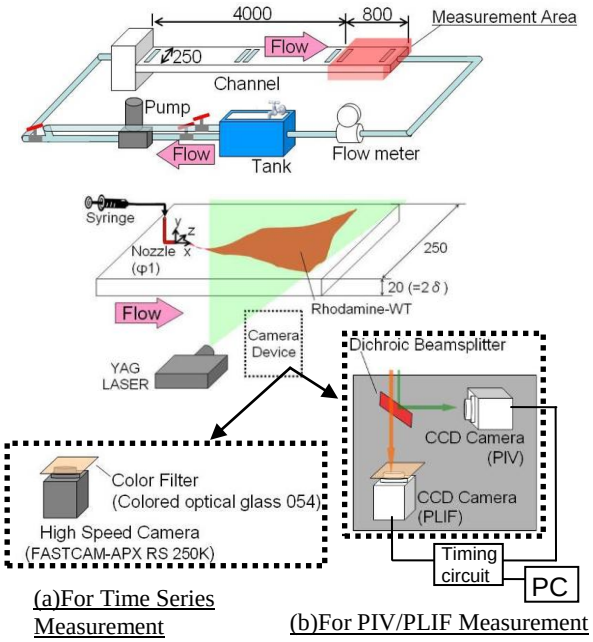

(a)For Time Series Measurement (b)For PIV/PLIF Measurement

Fig.1 Experimental Setup

channel flow was established in the channel, which had a rectangular cross-section 20 mm in height (2δ) with a 250 mm wide flume. It has an enough distance to approach the measurement area that had been fully developed and had no velocity gradient in spanwise distribution and the error range of root-mean-square values for the streamwise velocity was ±30% in the central region of the channel. These conditions imply a character of quasi-homogeneous turbulence in the (*x*, *z*) plane. The bulk Reynolds number was settled as 20000. The velocity field was measured by PIV (Particle Image Velocimetry) measurement.

In order to visualize the diffusion from the point source, PLIF (Planar Laser-Induced Fluorescence) measurement, which is widely used to obtain concentration fields (Webster et al., 2003; Motozawa et al., 2012) was performed in this research. The fluorescent dye was emitted from a nozzle located at the center of the channel. The nozzle had a 1 mm inside diameter and a 2 mm outside diameter. The emission velocity was controlled to 1.0 m/s by a syringe pump (kd Scientific210). The peak absorption of the fluorescent dye was about 532 nm and the peak emission was around 580 nm. An optical cutoff filter blocked the laser light and passed only the fluorescent light to the camera sensor. The laser was Nd: YAG laser and 0.6 mm thick was made by a cylindrical lens in the center of the channel (y^*=0)[1]. On the other hand, the PIV technique was applied to measure the velocity field. When we performed the PIV, we used the same laser with PLIF. Flo-Thene 20S was chosen as a tracing particle. The particle reflects the laser light and the velocity vector was analyzed using the captured images.

In this research, utilizing PLIF and PIV techniques,

[1]Superscript ( )* means normalization by half height of the channel δ.
For example, $x^*=x/\delta$, $y^*=y/\delta$ and $z^*=z/\delta$

Table.1 Conditions for each measurement

	PIV/PLIF measurement	PLIF time-series measurement
Test fluid	Water (25℃)	
Reynolds number	$Re = 2\delta U_b/\nu = 20000$	
Dye	Rhodamine-WT	
Color filter	HOYA: colored optical glass 054	
Laser	Nd:YAG	CW-YAG
Camera	Two CCD cameras	Photoron: FASTCAM-APX RS 250K
Frame rate	4 fps	1000 fps

we can carry out two kinds of experiments: time-series measurement of the concentration field, and simultaneous measurement of the concentration and the velocity field. Both experimental conditions are shown in Table 1. The former needs a camera device including a high-speed camera as shown in Fig. 1 (a). The resolution was high enough to resolve fine-scale eddies in the turbulent flow: the photographed area was 12.5δ × 12.5δ, which equals 1024 × 1024 pixels. The latter needs two CCD cameras synchronized by a timing circuit as shown in Fig. 1 (b). The reflected light from the tracing particle and the fluorescent light from the dye were split by a dichroic beam splitter. This made it possible to measure the concentration and the velocity field at the same time. The photographed area was 4.7δ × 4.7δ, which equals 2048 × 2048 pixels.

3. RESULT AND DISCUSSION

3.1. Characteristic Extraction

In order to perform a source estimation from an instantaneous turbulent diffusion field, it is necessary to understand the characteristics of the distance or period elapsing between an observation point and a source. Therefore, we tried to extract several characteristics which were valid for the source estimation.

3.1.1. Turbulent and molecular diffusion. In this section, we will introduce a result of the concentration and velocity field measured by the PIV/PLIF experiment. In Figure 2 (a), you can see 3 figures which enlarge a portion of instantaneous concentration distributions at x^*=10, 35, 60.

Our considerations about these figures are follows. First of all, we focused on the figure of x^*=10. This figure shows that a concentration plume which has a relatively high density presents here discretely. The plume has various scales L_{px}^* but it seems to be about L_{px}^* = 0.1 to 0.9 in the streamwise direction, and length in the spanwise direction L_{pz}^* was tiny as a resolution to L_{pz}^* = 0.8. Note that the largest plume scale nearly equals the integral scale L_I^*=0.7 in this flow. The dye did not spread enough in the

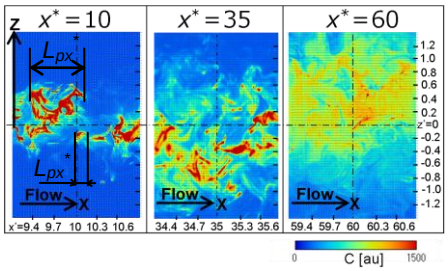

(a) Concentration fields

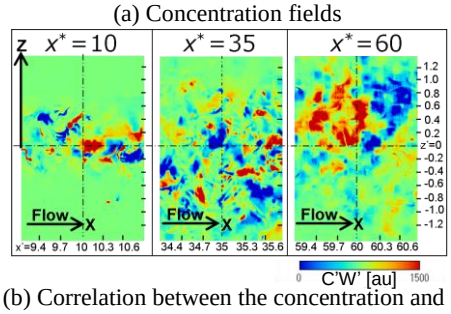

(b) Correlation between the concentration and velocity fields

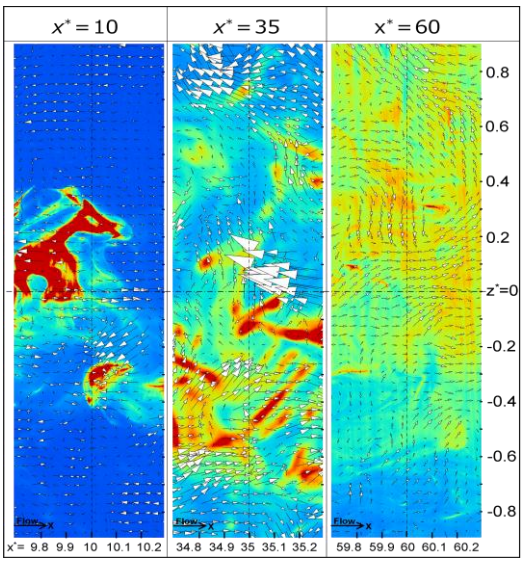

(c) Concentration and velocity fluctuation fields

Fig.2 Instantaneous concentration, velocity and correlation fields

spanwise direction and thus presents a locally-concentrated area. The shapes of these plumes are stretched like a filament due to turbulent diffusion.

Next, focusing on the figure of x^*=35, we can see that the plumes exist discretely, as seen in the figure x^*=10. A dye containing region is spread over a wide range in the z-direction because diffusion towards the spanwise distribution is advanced. It is also seen that the plumes are split due to a stretching effect by the motion of vortexes because many separated plumes indicate the filament shape. In other words, the larger plumes which were observed at x^*=10 had separated into smaller ones due to the turbulent diffusion effect.

In the more downstream region, x^*=60, a noticeable concentration plume cannot be observed. However, continuous distributions exist in the streamwise direction. Also, the high concentration region in the spanwise direction was spread more widely in this area.

Furthermore, you can see an instantaneous velocity and concentration field in Fig. 2 (c). In this figure, we can find that the plumes at x^*=10 have high contrast against the circumference field. The reason for this feature is that the dye had not diffused so much through molecular diffusion because it had not spent a long time reaching this region. The molecular diffusion has progressed to a more downstream region and the contrast of the concentration around the plume is getting low. In this way, due to the turbulent and the molecular diffusion, the overall width of the concentration plume became larger.

Considering these observations, it may be the key for the source estimation that a proportion of turbulent and molecular diffusion which affects the concentration distribution.

3.1.2 Meandering plumes. Generally in homogeneous turbulent flows, the mean concentration distribution in the spanwise direction shows a Gaussian distribution (Webster, 2007). This empirical relation is based on the assumption that the scalar is diffused by the random motion of turbulent eddies. This can be applied also in this research; a statistical distribution in the spanwise direction fits the Gaussian distribution, which mean value and the peak of the concentration locates z^*=0. However, in instantaneous distributions shown in Fig. 2(a), a coordinate in the z-axis direction where a peak concentration is located has fluctuated. An orbital of the dye can be seen to have meandered in the spanwise direction. The more downstream the observation area is, the smaller the deflection width is expected to be.

This fact is also a valid character of the source estimation that indicates the distance between an observation point and a source.

3.1.3 Correlation between concentration and velocity field. In order to obtain the relation between the concentration variation from the statistical distribution and velocity field, we investigate the correlation of concentration fluctuation C' and spanwise velocity fluctuation W' shown in Fig.2(b). In the upstream region, it is shown that a negative and positive correlation part appears alternately on a small scale in the streamwise direction.

Meanwhile, both negative and positive parts appear divided on a relatively large scale in the downstream area like x^*=60. Our assessment of these results is as follows. At x^*=10, the scale of the plume seems to be smaller than that of the velocity field. If the scale of the plume is smaller than that of the velocity field, the correlation distribution does not show a spatial gradient in the scale of turbulent eddies. The conceptual model is shown in Fig. 3 (a). This condition makes correlation values vary enormously. On the other hand, at x^*=60, turbulent and molecular diffusion advance and the contrast in the concentration field is more weakened and the size of the plume gets larger. As a result, the plume scale increases and shows stable distributions. This condition causes the

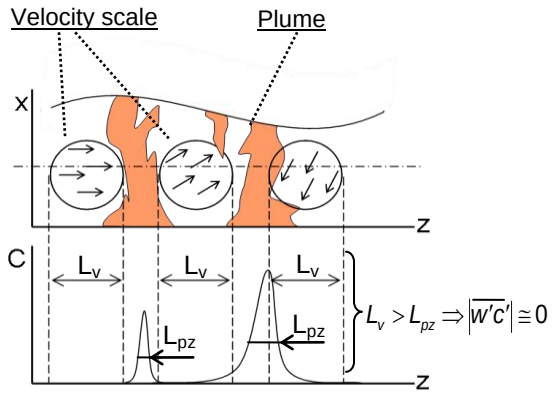

(a) upstream region (the velocity scales are bigger than the concentration scale)

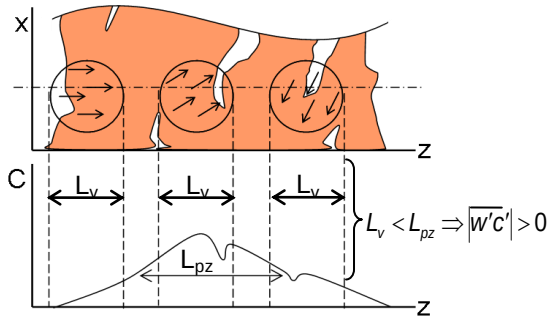

(b) downstream region (the concentration scale t are bigger than the velocity scales)

Fig. 3 Conceptual model of concentration and velocity fluctuation relation in upstream and downstream region

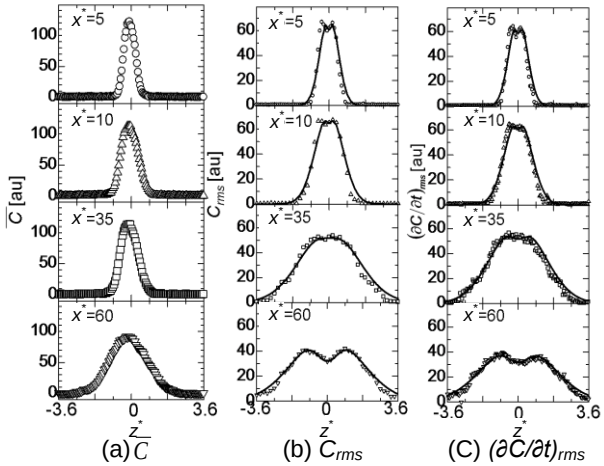

Fig.4 Statistical results for each analysis

number of regions which strongly correlate with concentration and the velocity field to increase in downstream regions.

Considering the correlation between the concentration and velocity field, we can find the size of the scales of the plume compared with that of the velocity field, which indicate a distance or period elapsing between an observation point and a source.

Table 2 Details of the data

	Large data	Statistical Approach Small data A	Instantaneous Approach Small data B
Number of stremwise locations	4	3	3
Number of spanwise Locations	400	5	400
Number of ensemble at single Location	1000	100	1
Total data size	1.6×10^6	1.5×10^3	1.2×10^3
Number of trial	-----	100	100

3.2. TRIALS FOR THE SOURCE PRESUMPTION

In this section, we will introduce two kinds of results of a source presumption method based on a concentration distribution measured by a PLIF experiment using a high speed camera.

3.2.1. Statistical Approach

First, we will introduce a simple trace back method using a statistical approach based on captured images. To analyze statistical datasets, we obtained a time-averaged dataset named 'large data', which contained 1000 sampling datasets at four different distances along the streamline (x^* = 5, 10, 35, 60) and 400 measurement points in the spanwise direction at each distance. We used it in order to obtain a relational expression between the distance from the emission point and the statistical results for several physical indexes. Thus, we calculated the distance from the source by applying the expression obtained from 'large data' to 'small data A'. This data included 100 sampling datasets for each distance (x^*=10, 35, 60) and only five points in the spanwise direction. Details of 'large data' and 'small data A' are summarized in Table 2. Utilizing these data, we performed the source estimation and checked the validity of this method.As the statistical datasets, we calculated their time-averaged concentration $\overline{C}$ or root-mean-square values C_{rms}, $(\partial C/\partial t)_{\mathrm{rms}}$ based on large data. The results are shown in Fig. 4. The time-averaged $\overline{C}$ is shown in Fig. 4(a), revealing that its distribution fits well with the Gaussian curve. As for C_{rms} and $(\partial C/\partial t)_{\mathrm{rms}}$, their spanwise profiles had two local maximums, given in Figs. 4 (b) and (c). Therefore, an approximate curve may be expressed by a superposition of different Gaussian distributions as shown in Eq. (1)

$$\Phi_i(z) = \frac{a_{i1}}{\sqrt{2\pi}\sigma^*_{i1}} \exp\left(\frac{-z^{*2}}{2\sigma^{*2}_{i1}}\right) - \frac{a_{i2}}{\sqrt{2\pi}\sigma^*_{i2}} \exp\left(\frac{-z^{*2}}{2\sigma^{*2}_{i2}}\right) \quad (1)$$

To decide the standard deviations and the coefficients of Eq. (1), a_{i1} and σ^*_{i1} were calculated to fit the distribution outside the local maximum value of Φ_i. Then, a_{i2} and σ_{i2} were chosen to fit the expression to the entire distribution of Φ_i. As a result, the expression that minimized the

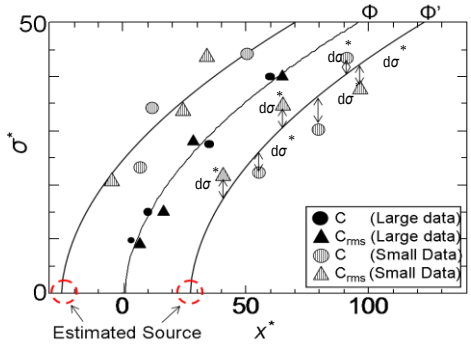

Fig.5 Conceptual model of statistical approach

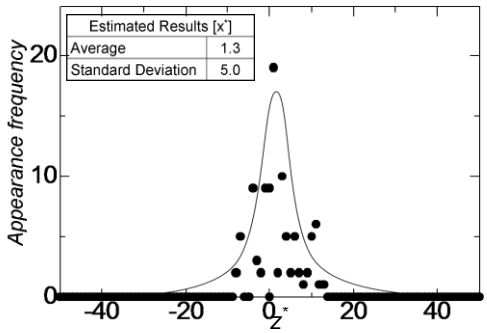

Fig.6 Result of statistical approach

difference from the statistical distribution could be selected. Actually, the approximation using two different Gaussian distributions was in good agreement with the measured values. According to Taylor's diffusion theory, the width of the concentration diffusion is proportional to one half the power of the distance from the source x^*. Considering this trend, both a and σ are summarized in Eqs. (2)-(4). Since no noticeable difference can be seen in the above coefficients regarding C_{rms} and $(\partial C/\partial t)_{\mathrm{rms}}$, we will focus especially on $\overline{C}$ and C_{rms}

$$\cdot \overline{C} \qquad \sigma^*_{11} = a_{11}\sqrt{x^*} \qquad a_{11} = 0.15 \qquad (2)$$

$$\cdot C_{rms} \qquad \sigma^*_{21} = a_{21}\sqrt{x^*} \qquad a_{21} = 0.23 \qquad (3)$$

$$\sigma^*_{22} = a_{22}\sqrt{x^*} \qquad a_{22} = 0.07 \qquad (4)$$

Using these equations, source estimation is performed by using 'small data A' to estimate the emission point in the short term. The data has five points of concentration information in the spanwise direction. By utilizing Eq. (1), the standard deviations σ'_{ij} which are required to predict the source can be calculated from small data[2].

They are approximated with $(x^*)^{0.5}$ by a linear relationship that has the same gradient a as Eqs. (2)-(4) and has a different x-intercept. The source is considered to be the x-intercept when an error E' shows the smallest value. A conceptual model of this method is shown in Fig. 5, and E' is shown in Eq. (5), (6).

$$d\sigma^{*k}_{i1} = \sigma^{*k\prime}_{i1} - \sigma^{*k}_{i1} \qquad (5)$$

$$E' = \sum_{k=1}^{3}\sum_{i=1}^{2}\frac{1}{a_{i1}}\sqrt{(d\sigma^{*k}_{i1})^2} \qquad (6)$$

[2] The value obtained from small data is indicated with superscript ( )'.

Table.3 Accuracy and deviation of estimated source position

	Error		Relative Error	
Instantaneous Approach	Bias, x^*_{est}	-1.72	x^*_{est}/L^*_x	0.049
	Deviation, $(x^*_{\mathrm{est}})_{\mathrm{rms}}$	10.8	$(x^*_{\mathrm{est}})_{\mathrm{rms}}/L^*_x$	0.31
Statistical Approach	Bias, x^*_{est}	1.3	x^*_{est}/L^*_x	0.037
	Deviation, $(x^*_{\mathrm{est}})_{\mathrm{rms}}$	5.0	$(x^*_{\mathrm{est}})_{\mathrm{rms}}/L^*_x$	0.14

Note that the variable number i changes from 1 to 2 because we are focusing on only $\overline{C}$ and C_{rms}. The superscript k=1, 2, 3 corresponds to the measurement locations x^*=10, 35, 60.This trial was repeated 100 times and the results are shown in Fig. 6. In this figure, you can see the frequency of the estimated source. An average and a standard deviation of x^*_{est} are defined in Eq. (7), (8).

$$\overline{x^*_{est}} = \frac{1}{N}\sum_{l=1}^{N} x^*_{est,l} \qquad (7)$$

$$(x^*_{est})_{rms} = \frac{1}{N}\sqrt{\sum_{l=1}^{N}(x^*_{est,l} - \overline{x^*_{est}})^2} \qquad (8)$$

The number of the trial N equals 100, which means the number of ensembles at a single location of the small data. As a result, values of relative errors were 0.037 for the average and 0.14 for the standard deviation. The distance criterion L_x^* equals 35 in this case.

3.2.2. Instantaneous Approach

In the previous section, we introduced the results of the statistical approach. In this section, you can see the results of the instantaneous approach. The difference between these methods is the size of the small data. To distinguish between the small data in the previous section and this section, we named it "small data B" in this section. The instantaneous data contain only one sampling dataset at three different distances along the streamline (x^* = 10, 35, 60) and 400 measurement points in the spanwise direction at each distance. Because of that, indexes such as mean value or RMS values cannot be calculated. Therefore, we calculate standard deviations of the concentration distribution of each instantaneous data.

As in the previous section, we supposed the width of the concentration diffusion was proportional to one half the power of the distance from the source x^*. Considering this trend, we presumed the source of diffusion from datasets obtained at x^* = 10, 35, 60 by applying the following expression.

$$\sigma_j = a_i\sqrt{x^*_j - b_i} \qquad (9)$$

Here, a_i was selected the a_{11} in Eq. (2) and b_i was decided by the least squares approximation that was applied to each dataset. The value of b_i was considered to be the location of the source as shown in Fig. 7. The result of estimations from 100 datasets is shown in Fig. 8. Though the predicted point must be at x^* = 0 ideally, the source of diffusion was estimated at x^*_{est}=-1.72 on average and had 10.8 (x^*) as a standard deviation. An average and a standard deviation of x^*_{est} have already been defined in Eq. (7), (8). Here, N, the number of the trial, equals 100.

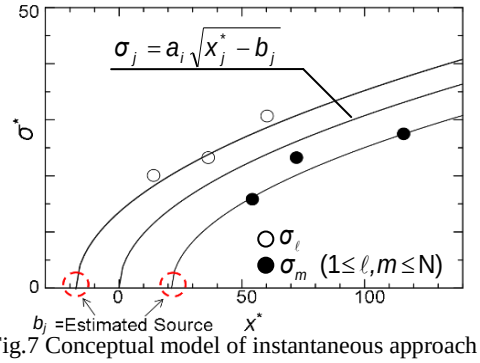

Fig.7 Conceptual model of instantaneous approach

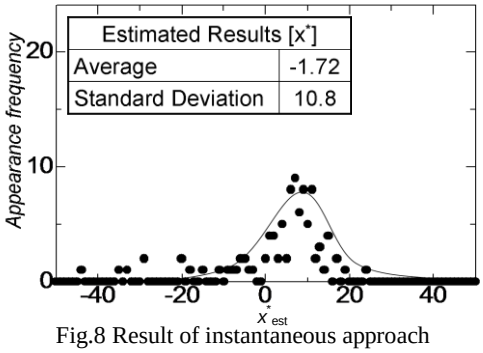

Fig.8 Result of instantaneous approach

Values of relative errors were -0.049 for the average and 0.31 for the standard deviation in the case that the distance criterion L_x^* equals 35.

The comparison of this result with the instantaneous one is shown in Table 3. Considering these results, it can be said that the statistical approach can perform source prediction with higher accuracy in the conditions that accompany quasi-homogeneous turbulence in a channel flow.

CONCLUSION

In this paper, we introduced the results of a PIV/PLIF simultaneous experiment. Considering the concentration and velocity field, and their correlation, we were able to find various experimental characteristics that indicated the condition of the diffused dye at different distances from the source: the condition of turbulent and molecular diffusion, the meandering of the plume and the size of the scales of the plume compared with that of the velocity field. Thus, PLIF time-series measurement was also performed. Utilizing the data from this, we tried two methods for the source estimation: an instantaneous approach and a statistical approach. As a result, the statistical approach leads that the position of the source was x^*=1.3 on average and its standard deviation was 5.0 (x^*). Also, the values of relative errors were 0.037 and 0.14, respectively. These results indicate higher accuracy compared with the instantaneous approach.

REFERENCES

Bagtzoglou, A., Dougherty, D. and Tompson, A., 1992, "Application of Particle Methods to Reliable Identification of Groundwater Pollution Sources", *Water Resources Management*, vol. 6, pp. 15-23.

Furuno, A., Chino, M. and Yamazawa, H., 2006, "Development of a Source Term Estimation Method for Nuclear Emergencies by Long-range Atmospheric Dispersion Simulation", *Trans. of the Atomic Energy Soc. of Japan*, vol. 5, pp. 229-240.

Islam, M., 1999, "Application of a Gaussian Plume Model to Determine the Location of an Unknown Emission Source", *Water and Soil Pollution*, vol. 112, pp. 241-245.

Kathirgamanathan, P., McKibbin, R. and McLachlan, R. I., 2002, "Source Term Estimation of Pollution from an Instantaneous Point Source", *Res. Lett. Inf. Math. Sci.*, vol. 3, pp. 59-67.

Motozawa, M., Kurosawa, T., Otsuki, T., Iwamoto, K., Ando, H., Senda, T. and Kawaguchi, Y., 2012, "PLIF Measurement of Turbulent Diffusion in Drag-Reducing Flow with Dosed Polymer Solution from a Wall", *J. of Thermal Science and Tech.*, vol. 7, pp. 272-287.

Webster, D. R., Rahman, S. and Dasi, L. P., 2003, "Laser-induced fluorescence measurements of a turbulent plume", *J. of Engineering Mechanics*, vol. 129, pp. 1130-1137

Webster, D. R., 2007, "Structure of turbulent chemical plumes," R. L. Woodfin (ed.), *Trace Chemical Sensing of Explosives*, John Wiley and Sons, New York, pp. 109–129.